J Intell Robot Syst (2013) 69:83–89
DOI 10.1007/s10846-012-9781-7

Energy Extraction from Onflow Inhomogeneity in the Spanwise Direction. A Theoretical Study

Vitaly Dmitriev · Patrick Jenny

Received: 27 August 2012 / Accepted: 30 August 2012 / Published online: 30 September 2012

Abstract Potential of energy extraction from onflow inhomogeneity in spanwise direction was investigated theoretically. Trajectory optimization was performed for a 5 meter span UAV with morphing capability as well as without it. Results show that energy extraction from inhomogeneity in spanwise direction is of little practical relevance compared to gust soaring. Morphing can be effectively used for drag reduction and stabilization while flying in a turbulent windfield.

Keywords Dynamic soaring · Trajectory optimization · Windfield simulation

1 Introduction

Energy extraction from wind inhomogeneity has been widely studied from a biological as well as from an engineering point of view. Cases treated include orographic wind [1], wind gusts [2] as well as vertical wind shear [3]. Even extreme cases like soaring in hurricanes were investigated [4].

V. Dmitriev (✉) · P. Jenny
Institute of Fluid Dynamics, Swiss Federal Institute of Technology, 8092 Zurich, Switzerland
e-mail: dmitriev@ifd.mavt.ethz.ch

P. Jenny
e-mail: jenny@ifd.mavt.ethz.ch

Using the example of the Knoller–Betz effect it should be noted that the timeline of efforts dedicated to examination and application of energy extraction shows gradual sobering as models became more and more sophisticated. The first very promising statements based on Lilienthals' polars [5, 6] had to be corrected after introduction of wake and instationary effects [7, 8] and experimental investigations [9, 10]. Gust soaring was found too challenging for a human pilot, but was applied for a UAV [11]. The resulting gain was by far not the one predicted originally by Knoller and Betz. Thus results presented here should be treated with care.

In this study the gust model will be refined by adding onflow inhomogeneity in the spanwise direction. Our goal is to investigate whether this refinement would allow perceivable gain for a plane with morphing capability.

2 Optimization Problem Setup

We solve a trajectory optimization problem to extract energy for a glider flying forward with negligible lateral shift. It is assumed that the wind history is known to the optimizer in advance. Effect of morphing is reduced to dynamic change of the lifting coefficient distribution along the wing.

2.1 Dynamic Model

The following ground-based coordinate system is employed: x-axis points ahead of the the aircraft, y-axis points starboard and z is aligned with the gravity vector. State variables are related to the plane dynamics and can be described by a 4-component vector $(v_x(t), v_z(t), P(t), \phi(t))^T$. The first two components are x- and z-components of the speed vector. The last two components denote rolling angular speed and roll angle. Effect of the lateral shift and change of yawing angle are neglected, whereas the pitching angle is included into the control vector (considerable control authority of the empennage is assumed). In aerodynamic computations we use body-based coordinate system x', y', z' having same orientation and placed at the gravity center of the aircraft.

2.2 Target Functional and Constraints

We seek to maximize the target functional

$$J = \frac{1}{T}\left[-mg\int_0^T v_z(t)\,dt + \frac{m}{2}\left(v_x^2(T) + v_z^2(T)\right)\right] \quad (1)$$

under initial and terminal boundary constraints:

$$\begin{aligned} v_x(0) &= 0 \quad v_x(T) \geq 0 \\ v_z(0) &= 0 \quad v_z(T) \leq 0 \\ P(0) &= 0 \quad P(T) = 0 \\ \phi(0) &= 0 \quad \phi(T) = 0 \\ \theta(0) &= 0 \quad \theta(T) = 0, \end{aligned} \quad (2)$$

where the maneuver duration T can be selected between 3.5 and 80 s.

Separate optimizations were done for a plane that can use dynamic morphing and for an optimized fixed wing plane. The latter case shall be referred to as "*conventional*" or "*non-morphing*". Fixed parameters are plane mass, rolling moment of inertia, wing area S and the viscous drag coefficient. Wing taper can be varied linearly with a limitation on the shortest chord. Twist for the conventional plane is an orthogonal sum of two components: the first one is elliptically distributed and the second one takes values between $-1°$ and $1°$ at $N = 19$ equidistantly spaced locations. Of all environmental parameters only the average windspeed U can be chosen by the optimizer between 3.0 m/s and 25 m/s.

Optimizer can define the dynamics of control variables by choosing them at $M = 39$ equidistant time instants in $(0, T)$. Morphing dynamics is controlled at the same N points as the twist and is reduced to a parameter called morphing angle of attack measured in grad. We assume that its sum with the aerodynamic pitch is linearly related to the lifting coefficient. Rate of change of the parameter is bounded by 5.0°/s. For the non-morphing wing case, ailerons are controlled to stabilize the roll angle. The pitching angle is controlled for both cases with the rate of change $|\theta'(t)|$ bounded by 8°/s.

2.3 Turbulence Model

It is assumed that the windspeed vector is always pointing in the x-direction and depends only on x and y coordinates. Following [12] its turbulent component u is modeled by a trigonometric expression with $K = 100$ terms:

$$u(x, y) = U + \sum_{i=1}^{K} \hat{u}_i \cos(\kappa_i y + \psi_i x + \varphi_i). \quad (3)$$

In this section we shall define the expressions for the (deterministic) numbers κ_i as well as for the (independently randomly chosen) numbers $\hat{u}_i$, $\psi_i^{(1)}$ and φ_i.

We start by choosing points $0 = d_0 < \ldots d_i < d_{i+1} < \ldots d_{K+1}$ in the wavenumber space. Difference to the usual modeling procedure is that in our case one has to model a big portion of the spectrum and the points have to be placed accurately. Eddies with lengthscale of a typical wingspan of a UAV are much smaller than the integral length scale. Energy spectrum shows the usual "5/3 behavior" in the inertial subrange [13] and due to its steepness one has to account for very large wavenumbers in order that the UAV would perceive the turbulence as an inhomogeneity in the spanwise direction. To achieve this task with limited amount of modes an inhomogeneous mesh was designed empirically with points $\{d_i\}_{i=0}^{K+1}$ being divided into three groups. As in [12] first 5 points are placed equidistantly

so that $\frac{\int_0^{d_5} E(\kappa)\,d\kappa}{\int_0^{d_{K+1}} E(\kappa)\,d\kappa} = 0.6$. The second group contains 50 points which are distributed such that $\frac{\int_0^{d_{55}} E(\kappa)\,d\kappa}{\int_0^{d_{K+1}} E(\kappa)\,d\kappa} = 0.95$ and $\int_{d_i}^{d_{i+1}} E(\kappa)\,d\kappa$ is constant for each $5 < i < 55$. The last 40 points are placed using the same principle to cover the last 2 % of the energy spectrum.

The Fourier modes are normally distributed zero mean random variables with variance defined by the turbulent energy spectrum E:

$$\langle \hat{u}_i^2 \rangle = 2\frac{\int_0^{\infty} E(\kappa)\,d\kappa}{\int_0^{d_{K+1}} E(\kappa)\,d\kappa} \int_{d_i}^{d_{i+1}} E(s)\,ds. \tag{4}$$

For each $1 \le i \le K$ wavenumber κ_i is the midpoints of $[d_i, d_{i+1}]$. Distributions of ψ_i and φ_i will be defined by fitting the correlations in two directions [13]:

$$\begin{aligned} &\langle u(x, y+r)u(x, y)\rangle \approx \langle u^2\rangle g(r) \\ &\langle u(x+r, y)u(x, y)\rangle \approx \langle u^2\rangle f(r), \end{aligned} \tag{5}$$

where $g(r)$ approximates $\frac{1}{\langle u^2\rangle}\int_0^{\infty} E(\kappa)cos(\kappa r)\,d\kappa$ and $f(r)$ satisfies

$$g(r) = f(r) + \frac{1}{2} r f'(r). \tag{6}$$

By solving Eq. 6 we find that ψ_i should have the probability density function

$$\mathcal{P}[\psi_i](s) = \frac{1}{\kappa_i}\left[\mathrm{rect}\left(\frac{s}{\kappa_i}\right) - \mathrm{tri}\left(\frac{s}{\kappa_i}\right)\right], \tag{7}$$

where rect and tri are rectangular and triangular hat-functions, respectively, having support $[-1, 1]$ and reaching value 1 at zero. To diminish dependence of left-hand side in Eq. 5 on coordinate (x, y), random numbers φ_i are chosen to be normally distributed with significant variance and zero mean, such that the characteristic functions are negligible at one.

2.4 Aerodynamic Model

The aerodynamic model is based on the quasi-stationary lifting line theory [14] with modifications to account for weekly inhomogeneous incompressible onflow. When modeling aerodynamics for the morphing case, solution of the Prandtl equation was omitted to save computational time.

An equidistant mesh $\{y_i\}_{i=0}^{256}$ with segment centers $\{y_{i-1/2}\}_{i=1}^{i=256}$ is introduced along the lifting line. All calculations are made in the segment centers, indices are used to discern approximations from original physical quantities. Model delivers approximation to aerodynamic force distribution $\{\bar{F}_i\}_{i=1}^{256}$ so that the total aerodynamic force equals $\sum_i \bar{F}_i$.

We assume that the wing is affected by lift, induced drag and the viscous drag. Lift and the induced drag are essentially defined by the onflow velocity, attached and trailing vorticity. Vorticity is spatially organized as a system of horseshoe vortices assigned to each segment $[y_{i-1}, y_i]$, $i = 1, \ldots, 256$ with vorticity lines stretching infinitely far away parallel to the x'-axis.

To obtain the vorticities $\{\Gamma_i\}_{i=1}^{256}$ associated with the horseshoe vortices, we need to know onflow speed, profile depth and lifting coefficient at the segment centers. Onflow speeds $\bar{\mathrm{u}}_i^{\infty}$ are obtained by using frozen turbulence approximation [13]. As it turned out that v_x have small variations for the resulting trajectory, one can simplify further:

$$\bar{\mathrm{u}}_i^{\infty} = -\begin{pmatrix} v_x(t) \\ 0 \\ v_z(t) \end{pmatrix} - \begin{pmatrix} u(Ut, y) \\ 0 \\ 0 \end{pmatrix}. \tag{8}$$

Profile depths d_i depend on the taper determined by the optimizer. Lifting coefficient is assumed to be linearly dependent on total onflow angle α^{aero}. The latter is assumed to be sum of the onflow pitch and the morphing angle. Morphing angle at each segment center is defined by interpolation from the N points where it is controlled. The vorticity is approximated as

$$\Gamma_i = 0.5\mathrm{d}_i|\bar{\mathrm{u}}_i^{\infty}|c_a'\alpha_i^{\mathrm{aero}}, \tag{9}$$

where c_a' is the inclination of the linear part of the lifting polar. By means of the Kutta-Joukowski theorem [14] lift distribution can be defined using a vector product:

$$\bar{F}_i^{\mathrm{lift}} = \rho\Gamma_i[\bar{\mathrm{u}}_{i,j}^{\infty}, (0, 1, 0)^T]. \tag{10}$$

Viscous drag force distribution acting on a wing segment is approximated by

$$\bar{F}_i^{\mathrm{visc}} = 0.5\rho\mathrm{d}_i(y_i - y_{i-1})c_{\mathrm{vd}}|\bar{\mathrm{u}}_{i,j}^{\infty}|\bar{\mathrm{u}}_{i,j}^{\infty}, \tag{11}$$

where the viscous drag coefficient $c_{\mathrm{vd}} = c_{\mathrm{vd}}(\mathrm{Re}_i, \alpha_i^{\mathrm{aero}})$ depends on the chord-based Reynolds number $\mathrm{Re}_i = \frac{|\bar{\mathrm{u}}_i^{\infty}|\mathrm{d}_i}{\nu}$ and on the total onflow angle α_i^{aero}. This dependence is modeled using the data for airfoils optimized in course of the CHIRP project [15] and can be seen in Fig. 1. Here, viscous drag coefficients are presented depending on two variables: lifting coefficient and angle of attack of the onflow. Two colored lines on the argument plane are the boundaries where stall is very likely to occur. The data is presented for $\mathrm{Re} = 7 \cdot 10^5$. For smaller Reynolds numbers the viscous drag is additionally amplified: $c_{\mathrm{vd}}(\mathrm{Re}_i, \alpha_i^{\mathrm{morph}}) = c(\mathrm{Re}_i) c_{\mathrm{vd}}(7 \cdot 10^5, \alpha_i^{\mathrm{morph}})$ where coefficient c is presented in the Fig. 2.

It is assumed that the tail is not affecting the aerodynamics of the plane and the fuselage contributes only via viscous drag:

$$\bar{F}^{\mathrm{fus}}_{\mathrm{visc.\ drag.}} = \frac{\rho}{2}\left(c^{\mathrm{fus}}_{\mathrm{vd}}(\mathrm{Re}) + \tilde{c}^{\mathrm{fus}}_{\mathrm{vd}}(\mathrm{Re})|\alpha^{\mathrm{fus}}|^3\right) S |\bar{\mathrm{u}}^{\infty}_{i,j}| \bar{\mathrm{u}}^{\infty}_{i,j}, \quad (12)$$

where α^{fus} is the fuselage angle of attack. Viscous drag coefficients are additionally increased for decreasing chord-based Reynolds numbers in the same way as for the wing.

Modeling of stall is reduced to specification of conditions where it is likely to occur and to avoidance of those for the resulting trajectory. Viscous drag coefficient is increased dramatically if strong separation is assumed so that such state becomes unattractive for the optimizer. Occurrence of stall is related solely to total onflow angle α^{aero} and to the aerodynamic pitch with boundaries presented in Fig. 1.

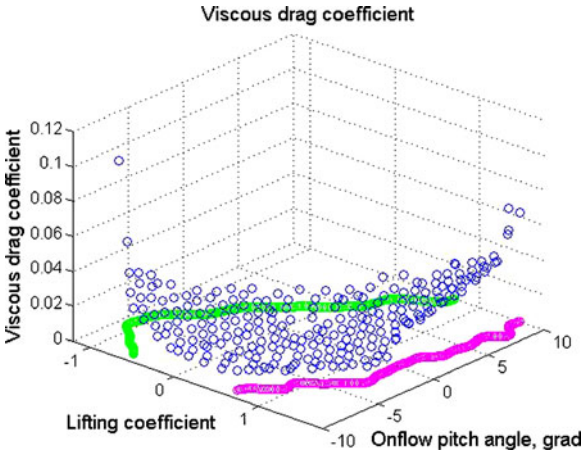

Fig. 1 Viscous drag coefficient

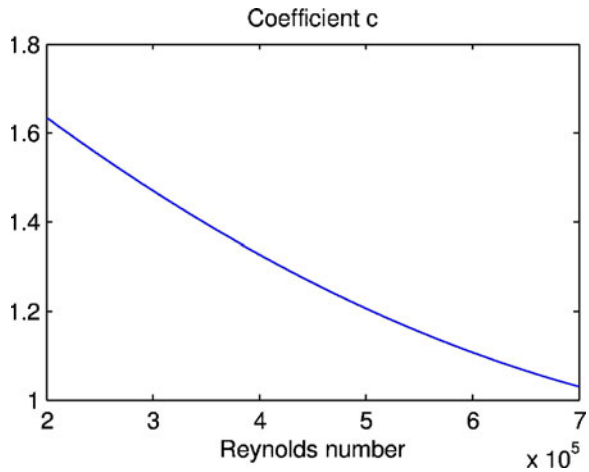

Fig. 2 Reynolds dependence of $c_{\mathrm{vd}}(\mathrm{Re}_i, \alpha_i^{\mathrm{morph}})$

Influence of the inhomogeneity is accounted for by eventually making these boundaries more stringent. For the morphing case we use the approach of Vandrey [16]. If one compares Prandtl equation cited in [16] with its pendant for the homogeneous case, it follows, that the extremities for the angle of attack should be multiplied with the coefficient $(1 + 2(\bar{\mathrm{u}}_i^{\infty} - <\bar{\mathrm{u}}^{\infty}>))^{-1}$. Here $<\bar{\mathrm{u}}^{\infty}>$ is the onflow average over the wingspan. This might lead to very pessimistic estimates and is assumed to give correct results only when $(\bar{\mathrm{u}}_i^{\infty} - <\bar{\mathrm{u}}^{\infty}>)$ is small. Another treatment of onflow inhomogeneity is due to Bausch [17] and it results in a model which would not make changes to the bounds and is applied when modeling conventional aircraft. Comparison made in [18] indicates, that no model is convincingly better, than another.

Induced drag originates from downwash $\bar{\mathrm{u}}^{\mathrm{dw}}$ calculated at $y_{i,j-1/2}$ using the Biot–Savart law:

$$\bar{F}_i^{\mathrm{ind.\ drag}} = \rho \Gamma_i \left[\bar{\mathrm{u}}_i^{\mathrm{dw}}, (0, 1, 0)^T\right]. \quad (13)$$

Practically calculation of the induced drag is made by multiplication of the vorticity vector by a downwash matrix. The latter has the Toeplitz property which allows to do matrix-vector multiplications by Fast Fourier Transform and save computational time [19, 20]. To make optimization faster

we abstain from calculation of the induced angle for the morphing case: estimation of the real angles of attack needed to obtain the desired values of Γ_i can be done aposteriorily. Of course, it can than happen that the resulting angle will be in the stall region, but this situation did not happen on practice. Besides, the evidence in [21] advises that the presence of downwash can broaden the region of allowed angles of attack. In case of conventional airplane the Prandtl equation is solved; inverse of the downwash matrix is stored before the start of the optimizations with its bisymmetric structure being taken into account. Experiments have shown, that for the matrix dimensions in question this is faster, than to use specialized algorithms for Toeplitz matrix inversion. Wake roll-up is not modeled: analysis in [22] suggests that it would have only minor effect.

Aerodynamic force distribution $\bar{F}_i = \bar{F}_i^{\text{lift}} + \bar{F}_i^{\text{ind. drag}} + \bar{F}_i^{\text{visc}}$, $i = 1, \ldots, 256$ defines the moments acting on the plane $\bar{M} = \sum_i [(0, y_{i-1/2}, 0)^T, \bar{F}_i]$.

3 Results

Optimization was done with *CAMTOS* algorithm from *GESOP* package developed by *ASTOS Solutions*. Collocation method was used with mesh dividing $[0, T]$ into $M + 1 = 40$ equidistant segments. Temporary change of control between mesh points was approximated by a piecewise linear function. For the state variables cubic splines were used. The state is thus not a solution to the governing ODE, but an approximation to it. Making it precise at a number of collocation points is one of the goals of the optimization. Collocation methods have an advantage in speed over shooting methods, but may deliver an inaccurate solution. It was observed, for instance, that if for the speed at which the plane flies through the frozen turbulence in Eq. 8 the real speed of the plane would be taken into account, the accuracy with mesh chosen would not be sufficient.

Table 1 Model parameters

Parameter	Value
Wingspan	5 m
Mass m	5 kg
Rolling moment of inertia	10 kg · m^2
Wing area	1.875 m^2
Smallest allowed chord	0.2 m
$c_{\text{vd}}^{\text{fus}}$	0.002 for large Re
$\tilde{c}_{\text{vd}}^{\text{fus}}$	0.0004 for large Re

Table 2 Trajectory parameters, wing morphing case

J	U	T	Smallest chord
−15.21 W	5.13 m/s	5.69 s	0.26 m
−13.97 W	8.68 m/s	7.55 s	0.27 m
−16.56 W	7.57 m/s	8.30 s	0.27 m

We have done optimizations for wind approximated by Eq. 3 for two different sets of parameters. The plane model is the same in both cases; the parameters are shown in Table 1. First, we modeled wind with E defined by Solari in [23] with surface roughness of 1.5 and shear velocity of 3.4 m/s (Table 2). Optimizations were done for three turbulent wind realizations, their statistics for mean and 68.2 %-confidence interval over the wingspan are plotted in Figs. 3, 4 and 5.

To show the main dependencies without aberrations caused by problems with optimization, we have chosen an atmospheric model with smaller amount of modes (Table 3); results are listed in Table 4. Those show that for the wing morphing case spacial inhomogeneity does not reduce the energy loss. Comparison of the two columns suggests that morphing can be effectively used

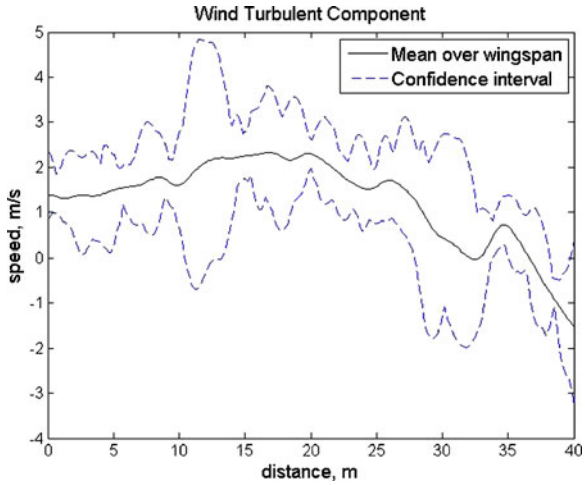

Fig. 3 Turbulent wind component the first experiment

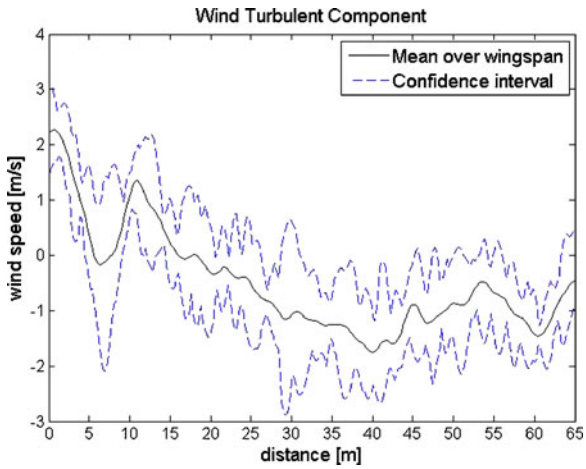

Fig. 4 Turbulent wind component for the second experiment

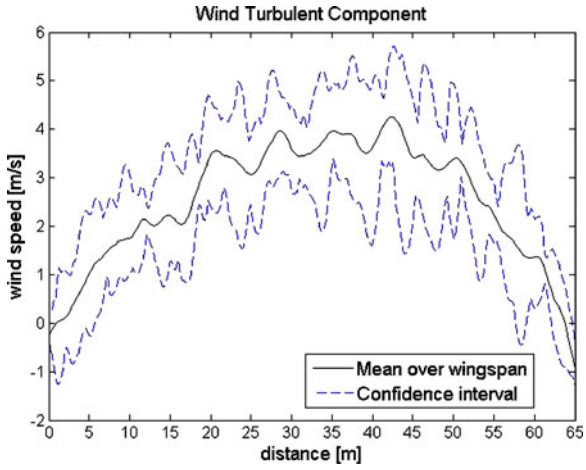

Fig. 5 Turbulent wind component for the third experiment

Table 3 Wind parameters

Parameter	Value
K	1 or 2
$\{u_1,\ u_2\}$	$\{2.0,\ 0.5\}$
$\{\kappa_1,\ \kappa_2\}$	$\{0.0,\ 0.63\}$
$\{\phi_1,\ \phi_2\}$	$\{0.0,\ 0.0\}$
ψ_1	0.021
ψ_2	0.05 or 0.1

Table 4 Results artificial wind model

Parameters	J, morphing	J, non-morphing
$K = 1$	−13.27 W	–
$K = 2,\ \psi_2 = 0.05$	−13.46 W	−16.55 W
$K = 2,\ \psi_2 = 0.1$	−13.43 W	−18.07 W

for drag minimization. But if we consider wider palette of wing planforms and broaden the boundaries for non-elliptic twist, the gap between results for two plane configurations will further decrease, this is especially true for the homogeneous atmosphere.

4 Conclusions and Further Work

As integral lengthscales of the atmospheric turbulence exceed 50 m, the energy extraction process does not benefit much from the inhomogeneity in the spanwise direction. Moreover, the timescales might not allow the plane to react even under the assumption that the whole wind history is known in advance. Additional complication is that the maneuvers leads to larger drag losses than for the optimal gliding case; not least because we impose boundary conditions 2 and consider small durations; it was shown in [24] that under such conditions the trajectory is not dictated by the point of optimal lift to drag ration. Though comparison with fixed-wing aircraft for turbulent atmosphere gives reasons to assert that morphing can effectively reduce drag losses. Our next goal is to further study condition granting energy gain by quantifying wind inhomogeneity for artificial atmospheric model and simplified plane dynamics.

Acknowledgements The authors would like to thank CHIRP project members Giulio Molinari, Manfred Quack, Francesco Previtali, Prof. Paolo Ermanni, Prof. Edoardo Mazza and Prof. Manfred Morari for inspiring discussions.

References

1. Langelaan, J.W.: Long distance/duration trajectory optimization for small uavs. In: AIAA Guidance, Navigation and Controls Conference (2007)
2. Langelaan, J.W.: Biologically inspired flight techniques for small and micro unmanned aerial vehicles.

In: AIAA Guidance, Navigation and Controls Conference. Honolulu, Hawaii, USA (2008)
3. Sachs, G.: Minimum shear wind strength required for dynamic soaring of albatrosses. Int. J. Avian Sci. **147**(1), 1–10 (2005)
4. Grenestedt, J., Montella, C., Spletzer, J.: Dynamic soaring in hurricanes. In: Proceedings of the ICUAS'12 Conference. Philadelphia, PA (2012)
5. Betz, A.: Ein Beitrag zur Erklärung des Segelfluges. Z. Flugtech. Mot.luftschiffahrt **3**, 269–272 (1912)
6. Knoller, R.: Die Gesetze des Luftwiderstandes. Flug- und Motortechnik (Wien) **3**(21), 1–7 (1909)
7. Birnbaum, W.: Der Schlagflügelpropeller und die Kleinen Schwingungen elastisch befestigter Tragflügel. Z. Flugtech. Mot.luftschiffahrt **15**, 128–134 (1924)
8. Durand, W.F. (ed.): Aerodynamic Theory. Springer, Berlin (1935)
9. Jones, K.D., Doring, C.M., Platzer, M.F.: Experimental and computational investigation of the Knoller–Betz effect. AIAA J. **36**, 1240–1246 (1998)
10. Koochesfahani, M.M.: Vortical patterns in the wake of an oscillating airfoil. AIAA J. **27**(9), 1200–1205 (1989)
11. Patel, C.: Energy extraction from atmospheric turbulence of improve aircraft performance. Ph.D. dissertation, Stanford University, California, USA (2007)
12. Fung, J.C.H., Hunt, J.C.R., Malik, N.A., Perkins, R.J.: Kinematic simulation of homogeneous turbulence by unsteady random Fourier modes. J. Fluid Mech. **236**, 281–318 (1992)
13. Pope, S.B.: Turbulent Flows. Cambridge University Press, Cambridge (2000)
14. Katz, J., Plotkin, A.: Low-Speed Aerodynamics, 2nd edn., Ser. Cambridge Aerospace Series. Cambridge University Press, Cambridge (2001)
15. Molinari, G., Quack, M., Dmitriev, V., Morari, M., Jenny, P., Ermanni, P.: Aero-structural optimization of morphing airfoils for adaptive wings. J. Intell. Mater. Syst. Struct. **22**, 1075–1089 (2011)
16. Vandrey, F.: Beitrag zur theorie des tragflügels in schwach inhomogener parallelströmung. Z. Angew. Math. Mech. **20**(3), 148–152 (1940)
17. Bausch, K.: Auftriebsverteilung und daraus abgeleitete grössen für tragflügel in schwach inhomogenen strömung. Luftfahrtforschung **16**, 129–134 (1939)
18. Seidel, M.: Der einfluss eines geneigten strahles auf das strömungsfeld in der umgebung eines leitwerks sowie auf dessen luftkraftbeiwerte. Teil II: Literaturübersicht. Deutsche Forschungsanstalt für Luft- und Raumfahrt, Braunschweig, Tech. Rep. 69/3 (1962)
19. Voevodin, V.V., Tyrtyshnikov, E.E.: Computational Processes with Toeplitz Matrices. Nauka (1987)
20. Golub, G.H., van Van Loan, C.F.: Matrix Computations, 3rd edn. John Hopkins University Press, Baltimore (1996)
21. McCormick, B.W.: Aerodynamics, Aeronautics, and Flight Mechanics, 2nd edn. Wiley, Canada (1995)
22. Smith, S.C.: A computational and experimental study of nonlinear aspects of induced drag. National Aeronautics and Space Administration, Ames Research Center, Moffet Field, California, NASA Technical Paper 3598 (1996)
23. Solari, G.: Gust buffeting. I: Peak wind velocity and equivalent pressure. J. Struct. Eng. **119**(2), 365–382 (1993)
24. Willis, D., Bahlman, J., Breuer, K., Swartz, S.: Energetically optimal short-range gliding trajectories for gliding animals. AIAA J. **49**, 2650–2657 (2011)